Droplet Asymmetry and Wetting Dynamics on Irregularly Roughened Surfaces

Kewei Shi,[1] Justin Elms,[2] Xili Duan,[1, a)] and Kristin M. Poduska[2, b)]

[1)]*Faculty of Engineering and Applied Science, Memorial University of Newfoundland, St. John's, NL, A1B 3X5 Canada*

[2)]*Department of Physics and Physical Oceanography, Memorial University of Newfoundland, St. John's, NL, A1B 3X7 Canada*[c)]

(Dated: 7 December 2020)

Abstract: This study illustrates pervasive challenges in studying wetting dynamics, including dynamic contact angles, on irregularly roughened surfaces. We demonstrate that asymmetric water droplet shapes occur more than than 50% of the time during static and dynamic contact angle measurements on sandblasted Zn-plated stainless steel with a polymeric overcoat. The pinning that causes the asymmetric drop shape distortion on horizontal surfaces also influences the sliding behavior on inclined surfaces. These effects lead to a poor correlation between the measured dynamic contact angles and the observed sliding angles (critical tilt angles). Our work emphasizes that large variations in the values of these dynamic wetting parameters are inherent to the heterogeneity of the surface roughness, and thus they limit the usefulness of standard dynamic wetting criteria. These findings have implications for academic and industrial research focused on making coated materials that have consistent wettability properties throughout their usage life cycle.

[a)]Electronic mail: xduan@mun.ca; www.engr.mun.ca/~xduan/

[b)]Electronic mail: kris@mun.ca; www.physics.mun.ca/~kris/

[c)]Current affiliation for J. Elms: College of the North Atlantic, St. John's, NL, A1C 5P7 Canada

I. INTRODUCTION

Non-wetting surfaces are studied in many disciplines of engineering and science because of the wide range of applications. For offshore infrastructure, paints are widely used to protect stainless steel from the salt and water that is inherent in marine environments. Some of these paints are hydrophobic to make the surfaces of the structures into non-wetting surfaces. However, paint wears quickly under these circumstances, making it costly and time-intensive to repair or reapply. It is intriguing to consider whether such stainless steel surfaces could be roughened to improve their hydrophobicity and overall durability.

Materials with high surface energies, such as metals, must often use a combination of coatings and roughness to achieve superhydrophobicity.[1–10] In general, rough surfaces allow air to become trapped between the solid and liquid which can lead to non-wetting behaviour, and can often be described by either the Wenzel or Cassie-Baxter models.[11–15] A great deal of work has been conducted for developing regularly patterned surface structures that are superhydrophobic.[9,10,12,16–20] Surface features such as channels, pillows and hierarchical structures[18] have been produced from fluorocarbons, silicon, copper, and zinc.[1,3,8–10,12,16–18,21,22] Although patterned surfaces with air gaps can be effective in reducing direct contact with water,[4,9,12,16–20] they are not easily produced on an industrial scale.[3]

Sandblasting is widely used in industry for preparing metal surfaces before painting, and it is readily applied on a large scale. Unlike intentionally patterned surfaces, sandblasting produces surfaces with irregular roughness, which has not been studied as intensively in the wettability literature.[2] However, investigations of the apparent contact angles on irregularly roughed silicon surfaces show that the Wenzel (fully wetting) and Cassie-Baxter (partial wetting) models do not adequately explain wetting behaviors.[23] Other work identified difficulties in quantifying dynamic wetting behaviour, demonstrating that apparent static contact angles alone are not sufficient to characterize randomly roughened surfaces, and that sliding angles and contact angle hysteresis data are needed.[24]

This study emphasizes that standard metrics for dynamic wetting behaviour, including dynamic contact angles, are not sufficient to study water on surfaces with irregular roughness. To do this, we report details of droplet shape variations on coated sandblasted steel, based on advancing and receding apparent contact angle measurements, and while varying the incline angle of the surface on which the drop sits. We demonstrate that asymmetric water droplet shapes occur more than than

50% of the time during static and dynamic contact angle measurements on sandblasted Zn-plated stainless steel with a polymeric overcoat. We identify droplet pinning and depinning events, and we explain why this leads to significant inherent complications in the measure of dynamic wetting behaviour on irregularly roughened surfaces. The pinning that causes the asymmetric drop shape distortion on horizontal surfaces also influences the sliding behavior on inclined surfaces. These effects lead to a poor correlation between the measured dynamic contact angles and the observed sliding angles (critical tilt angles). Our work emphasizes that large variations in the values of these dynamic wetting parameters are inherent to the heterogeneity of the surface roughness, and thus they limit the usefulness of standard dynamic wetting criteria. These findings have implications for academic and industrial research focused on making coated materials that have consistent wettability properties throughout their usage life cycle.

II. EXPERIMENTAL METHODS

A. Materials

Two primary test samples (both 30 $\times$ 30 $\times$ 0.8 mm stainless steel tiles, SAE 630/17-4, McMaster-Carr) were roughened with either 100 μm or 250 μm Al_2O_3 blasting media by using a Vaniman Problast micro-abrasive sandblaster. These are denoted as Sample 100 and Sample 250, respectively. In both cases, the blast pressure was kept constant at 100 psi while the nozzle tip was held 1 cm from the target surface. After sandblasting, the surface was coated with a Zn electrodeposit followed by stearic acid coating using a procedure that is described in detail elsewhere.[8] This surface treatment decreases the surface energy and increases hydrophobicity. Representative surface images were obtained with a scanning electron microscope (SEM, model FEI MLA 650F) using secondary electron imaging.

Additional stainless steel samples were used to collect more data for our pinning studies. In these cases, 100 to 1200 grit sandpapers were used to roughen 30 $\times$ 30 $\times$ 0.8 mm stainless steel, abraded in many different directions to randomise the surface profiles. The substrate was then immersed in Aculon for 20 minutes to reduce wettability. The substrates abraded with coarser sandpapers had higher apparent static contact angles.

B. Dynamic contact angle measurements

A contact angle measuring system (OCA 15EC, DataPhysics) in Figure 1 was used to characterize dynamic contact angles for droplets of ultrapure water (Barnstead, 18.2 MΩ·cm). The measurement system consisted of a backlit staging area, a software-controlled liquid dosing system, and a camera USB-Wide-VGA camera, maximum resolution 752 × 480 pixel, 6× optical magnification, distortion is smaller than 0.05%, maximum sampling rate 15 fps). The syringe-based dosing system used a BD PrecisionGlide 26 G × 1/2 hypodermic needle (diameter = 0.45 cm).

In this study, we measured dynamic contact angles using two different methods, as shown in Figure 2. For horizontal surfaces, the dynamic condition was met by volume modification (Figure 2a): θ_A and θ_R correspond to contact angles for the maximum and minimum droplet volumes, respectively. For the sliding droplet method (Figure 2b), the surface was tilted until the droplet began to slide ($\theta_t c$), at which point the advancing (θ_a) and receding (θ_r) contact angles were measured.

All substrates were cleaned with deionized water for 10 minutes and dried prior to affixing to the tilted base. For volume modification experiments, we used manual needle and sample placement to place needle close to – but not touching – the sample surface. Then, the user-defined volume of water (typically 20 µL) was expelled from the needle to form a droplet; the needle was retracted from the droplet before measuring the apparent contact angle. While resting on the substrate, a droplet's volume was doubled at the user-defined dosing rate (typically 2 µL/s); this is the advancing phase with a maximum contact angle θ_A. Once the droplet reached its maximum volume, there was a 2 second pause, followed by a volume reduction at the same user-defined rate until the droplet reached the initial volume; this is the receding phase, with minimum contact angle θ_R. When first deposited onto the surface, the drops often slid to a pinning site near the needle. The surface would then have to be reoriented so that the needle was centred in the droplet. Once the measurement began, the contact line would usually advance more in one direction. We tracked the shape change during the entire process, recording videos with frames that could be analyzed individually.

For sliding experiments, the camera tracked the shape and position change of the droplet (20 µL) as the substrate incline angle was gradually increased from 0 degrees (level) to the sliding point ($\theta_t c$, critical tilt angle).

C. Data processing and fitting

The software suite that accompanies the contact angle measurement system (SCA 20, Data-Physics) is designed to analyze droplet contact angles, volume, and base diameter automatically using the live view captured by the camera.

The contact angles of the droplet on the advancing (θ_A) and receding (θ_R) sides were measured manually, as well as the incline angle of the substrate (θ_t) based on images, as shown in Figure 2b. We saved images and, if necessary, manually rotated the images to make the inclined surface "flat" so the software can measure the contact angle on the left and right sides; we also compared the software fits with our own manual fits. Ellipse fitting is the most physically representative; unpinned droplets should be symmetric, and gravity will flatten their shape.

III. RESULTS AND DISCUSSION

A. Surface characterization

Figure 3 shows representative SEM images of the sandblasted surfaces used for our studies, both before and after coating. These images are for substrates used for sliding experiments; similar preparations were used for samples in the volume modification experiments. Features on all surfaces are very irregular, as expected, due to the sandblasting pre-treatment. The coated surfaces (Figure 3b,d) appear to have more rounded surface features than the as-blasted substrates (Figure 3a,c). It is not possible to assess the height of surface features based on grey scale differences in these SEM images, since the contrast is not based on heights but rather on the number of secondary electrons collected at the detector. We note that other instruments that are well-suited to assessing surface roughness (such a profilometer or atomic force microscope) are inappropriate for our samples because their mechanical probes cannot track intricate surface topography such as undercuts and steep features.

The lateral scale of the surface features shown in Figure 3 ($\sim$10-100 μm) is significantly smaller than a typical drop diameter in our experiments ($\sim$2 mm). Furthermore, our droplet diameters are less than the maximum capillary length for water under our experimental conditions. To calculate this, we used the gravitational acceleration (9.8 m/s^2) and a temperature of 20 °C to give a water density = 998 kg/m^3. Taking surface tension of water to be 72.8 $\times 10^{-3}$ N/m, we find a maximum capillary length $\lambda_c = \sqrt{\gamma/(\rho g)}$ = 2.7 mm.

B. Volume-modified droplets (horizontal surfaces)

We performed more than 300 dynamic contact angle measurements on horizontal (not inclined) roughened surfaces using volume modification. A representative example of the volume-dependent contact angle values are presented in Figure 4a. We note that apparent contact angles are in the superhydrophobic regime, which means that the contact area between the droplet and the surface is significantly smaller than the maximum droplet diameter. This means that we use only side-on views of the droplets; a top-down view would not allow us to see the contact region between the droplet and the surface. The contact angle values in Figure 4a are calculated from the average (left and right sides) of elliptical fits to the droplet's contour. More examples of the data are included as Electronic Supplementary Material.

Droplet pinning and depinning cause discontinuities in several aspects of the droplet characteristics during a volume modification experiment. This affects the length of the contact line between the droplet and the surface, as well as the contact angle. A pinned droplet will have a fixed contact line length, even as the droplet volume increases. Once the droplet depins, there is a discontinuous jump in the length of the contact line, which is concurrent with a discontinuous decrease in the droplet contact angle. Both of these manifestations of droplet pinning create challenges for measuring dynamic contact angles.

Figure 4b shows a droplet that advances preferentially to the right because the left side of the droplet is pinned. In some instances, the advancing direction changed during measurement, signifying that there was more than one pinning site within a single droplet diameter. Contact angles varied by 50° or more for identical volume droplets, and nearly all droplets exhibited asymmetric contact lines during dynamic measurements.

Given that pinning caused challenges for automated fits to droplet images, we investigated whether we could evaluate the quality of a measurement by comparing the calculated volume change to the actual droplet volume, based on the fact that we used constant dosing rates. The fitting software calculated droplet volume based on the contact line (solid-liquid contact) length and the contour of the air-droplet interface. Since both of these components show discontinuities during pinning events, the resulting volume calculation is extremely sensitive to pinning events. For example, the actual volume changes as a function of time were smooth and symmetrical, with initial and final volumes nearly equal. Figure 5a shows calculated volume data that looks like what we expect. In contrast, the calculated volume data shown in Figure 5b contains irregular dips and

peaks that are not representative of the droplet's true volume change. This was a sign that the contour fits did not capture the droplet's shape well, and that we should not trust the contact angles resulting from these fits.

Our idea to use calculated volume data as a screening approach is not standard, but it is very helpful for identifying when catastrophic droplet pinning occurs. It also elicited some surprising results.

We applied a threshold for a smooth volume change trend to more than 300 different volume-modified droplets, to then sort them into groups of acceptable and unacceptable measurements. A collection of representative examples are included in Electronic Supplementary Material. Surprisingly, we found no relation between the asymmetry of the left and right contact angles or the smoothness of the calculated volume change trends. However, we did find other useful information.

First, we determined that automatic fits themselves are not the root of the problems in fitting droplet contours. We investigated a range of different automated fitting rates ranging from from 1-10 s^{-1}, as shown in Table I. A collection of representative examples of the raw data are also included in Electronic Supplementary Material. Slower measurement rates were more frequently acceptable, with anything faster than 5 s^{-1} being equivalent. However, even in the best cases, less than 50% of the measurements met our criteria for acceptable results. We could boost the success rates by using smaller droplet volumes, or by using faster dosing rates. However, acceptable measurements never crossed the 60% threshold.

We were quite surprised that the acceptance statistics did not improve when we moved to manual fits instead of automated fits. The reason for this we attribute to droplet pinning. Even using these best practices, much of our contact angle data was still unusable with either automatic or manual fits. We conclude that this is related to catastrophic droplet pinning, which is (unfortunately) a common issue for randomly roughened surfaces.

C. Sliding droplets (inclined surfaces)

For inclined hydrophobic surfaces, we expect that the droplets will have asymmetric contact angles due to the effect of gravity (see Electronic Supplementary Material for more details). However, based on what we learned from horizontal experiments on our irregularly roughened surfaces, we expect an additional component to the droplet asymmetry as a result of pinning. In our experi-

ments, we recorded the critical tilt angle θ_{tc} droplet begins to slide, as well as the advancing (θ_a) and receding (θ_r) contact angles of the droplet just before sliding occurs. We demonstrate this by comparing our sliding data to a commonly used (Furmidge) model,[25] and we show that this simple model is not sufficient to explain our data.

This gravity-induced effect of pinning is clearly visible in our data. Figure 6 shows a representative example of how droplet contact angles change on a coated substrate as the tilt angle increases. The advancing angle (θ_a) stays nearly constant as the substrate tilt angle (θ_t) is increased from 0 to 15 $^\circ$. However, the receding angle (θ_r) changes significantly. These trends are qualitatively explained by free-body diagrams (provided in Electronic Supplementary Material) and they also agree well with the findings of others.[26]

There is another striking distinction between the trends we see in the advancing and receding contact angle data. The statistical uncertainties of advancing and receding angles, as represented by the error bars on data points in Figure 6, are different: those for advancing contact angles are significantly larger ($\pm 2.4^\circ$) than those for the receding contact angles ($\pm 0.1^\circ$). These fluctuation differences are not an artifact of poor droplet image fitting parameters, but rather they appear to be a result of inherent asymmetries in droplet pinning on these irregularly roughened surfaces.

Going beyond the magnitude of contact angle fluctuations, there are several substrate tilt angles at which θ_r changed rapidly between successive frames. These points are labelled “jumping points" and circled in Figure 6. An image of the droplet at the first jumping point (Figure 7a) shows that part of the droplet depins, but does not yet roll. To accommodate this depinning, the length of the base of the droplet decreases slightly ($\Delta D = 0.03$ mm). We note that this distance ΔD is substantially larger than the scale of the surface roughness (Figure 3), and that the uncertainty in all of our ΔD values are $\sim 5\%$. An image of the droplet at the second jumping point (Figure 7b) corresponds to the incline angle at which the droplet begins to slide. In this case, the contact points between the surface and the droplet move on both ends of the droplet with similar magnitudes: the leading edge advances by $\Delta D_a = 0.05$ mm , while the receding edge advances by $\Delta D_r = 0.06$ mm.

D. Comparison with the Furmidge model

For the sliding drop experiments, we applied a simple (Furmidge) model[25] to demonstrate that the droplet pinning that occurs on our irregularly roughened surfaces introduces an additional asymmetry to droplets on inclined surfaces.

Numerous studies by others have shown that droplet size, the degree of substrate wettability, adhesion between droplet and substrate, and surface roughness can each affect the sliding behaviour of a water droplet.[27–31] In ideal cases, the critical tilt angle is proportional to the difference between the cosines of the dynamic advancing and receding contact angles, based on a simple relation introduced by Furmidge:[14,25,32]

$$\frac{mg\sin\theta_{tc}}{w} = \gamma_{\mathrm{LV}}(\cos\theta_r - \cos\theta_a). \tag{1}$$

Here, θ_{tc} is the critical tilt angle at which the droplet slides, m is the droplet mass, g is the acceleration due to gravity, w is the drop width, γ_{LV} is the liquid-vapour surface tension, and θ_r and θ_a are the receding and advancing contact angles, respectively. The combined $mg\sin\theta_{tc}$ term is the component of the gravitational force that causes the drop to move. Figure 8 shows that there is poor agreement between our experimental data and this model. All experimental data show a higher critical tilt angle than Equation 1 would predict. There is no significant difference in the results between the two samples, even though they were roughened with different sizes of sandblasting media.

Previous work by others has shown that the Furmidge relation does not apply well to many surface and liquid combinations.[29,33] For example, one report finds that advancing and receding contact angles at the sliding point (critical tilt angle) are comparable to the volume-modified contact angles.[34] Other reports highlight high uncertainty estimates (50-60%) while using the sliding method to determine advancing and receding contact angles.[24,29] The Furmidge model is extremely simple, and does not account for any effects due to surface roughness. It is widely known that surface roughness can introduce air pockets in features that are too small for water to wet completely. More nuanced models for dynamic wettabilities of a water droplet on the roughened surface do exist. One combines the concept of partial surface wetting due to air pockets (Cassie-Baxter wetting) with the Furmidge model.[35] Other models have been developed to explain the dynamic behaviour of droplets, including sliding/sliding angles and maximum droplet radius while sliding on either rough or smooth surfaces.[36,37] These studies show that surface roughness significantly affects the sliding angles on superhydrophobic surfaces. Even so, none of these models are appropriate if droplets are asymmetric.

We note that there are many models that correlate wettability with surface roughness.[2] However, surfaces such as ours have roughness values that vary depending on the length scale of the measurement area. Quantification of multi-scale roughness is described in the literature, but it

does not mesh well with wetting models, especially when pinning is the dominant effect (as it is in the case of our samples). This is because it is not clear in the field exactly what features – and which length scales – ultimately control pinning behaviour. This is particularly challenging on surfaces with irregular roughening where there can be features with high asperities that would not be apparent by using standard spatially averaged surface roughness values.

IV. CONCLUSIONS

Our dynamic contact angle data illustrate common problems inherent to the study of wetting dynamics on randomly roughened surfaces, which is a topic relevant for large-scale industrial applications of wetting that are important over the life cycle of a material.

Droplet shapes on our irregularly roughened surfaces varied immensely due to severe droplet pinning. For dynamic contact angles measured on horizontal surfaces through volume-modified droplets, asymmetric drop shapes contributed directly to poor data automatic and manual data fits to droplet contours. We used these deviations to evaluate the quality of the data fits. Data quality improved with decreasing drop size. This result is beneficial to those studying realistic systems where small droplets come from precipitation, ocean spray, or other water sources. Other factors, such as dosing and measurement rates, also affected data fit quality. The most accurate fits were attained using higher dosing rates and lower fitting attempt rates. For droplets on inclined versions of the same irregularly roughened surfaces, nearly all droplets adhered to these surfaces, even though contact angles were in the superhydrophobic regime (~150°). This result could not have been explained by the simple Furmidge model that relates sliding angle to volume-modified contact angles. These difficulties were not limited to our sandblasted and coated steel: wetting behavior of other roughened metals and plastics (shown in Electronic Supplementary Material) showed similar problems with pinning.

We do not propose a more complicated empirical model to fit our data. Instead, we point out that we should not expect empirical models to be generalizable, or to hold for surfaces with irregular rough features. Moving forward, we suggest that future studies that involve contact angle assessments on surfaces adopt the following best practices:

1. Report dynamic advancing and receding contact angles, since apparent static contact angles alone are not sufficient.

2. Include images of the droplets and their fits, to show how droplet asymmetry was addressed.

By reporting these kinds of data together, authors can ensure that future researchers can compare wettability studies in a more informed way. These findings are relevant not only for metals, but could also be applied to studies of other coated solid surfaces.

ACKNOWLEDGMENTS

The authors thank Petroleum Research Newfoundland & Labrador (PRNL) Grant C15-03 for financial support for this research. The authors declare no conflicts of interest.

ELECTRONIC SUPPLEMENTARY MATERIAL

A PDF file contains additional details about gravitational effects on tilted droplets, representative raw data for volume-changed droplets, more data for droplets on tilted surfaces.

REFERENCES

[1]Roach P, Shirtcliffe NJ, Newton MI. Progess in superhydrophobic surface development *Soft Matter.* 2008;4:224.

[2]Kubiak KJ, Wilson MCT, Mathia TG, Carval P. Wettability versus roughness of engineering surfaces *Wear.* 2011;271:523–528.

[3]Shirtcliffe NJ, McHale G, Newton MI, Chabrol G, Perry CC. Dual-Scale Roughness Produces Unusually Water-Repellent Surfaces *Adv. Mater.*. 2004;16:1929–1932.

[4]Pham DC, Na K, Piao S, Cho IJ, Jhang KY, Yoon ES. Wetting behavior and nanotribological properties of silicon nanopatterns combined with diamond-like carbon and perfluoropolyether films *Nanotechnology.* 2011;22:395303.

[5]Boinovich LB, Emelyanenko AM, Ivanov VK, Pashinin AS. Durable icephobic coating for stainless steel *ACS Appl. Mater. Interfaces.* 2013;5:2549–2554.

[6]Steele A, Nayak BK, Davis A, Gupta MC, Loth E. Linear abrasion of a titanium superhydrophobic surface prepared by ultrafast laser microtexturing *J. Micromech. Microeng.*. 2013;23.

[7]Yang X, Liu X, Lu Y, et al. Controlling the Adhesion of Superhydrophobic Surfaces Using Electrolyte Jet Machining Techniques *Sci. Rep.*. 2016;6.

[8]Gao B, Poduska KM. Electrodeposited Zn for Water-Repellent Coatings *J. Electrochem. Soc.*. 2018;165:D472–D476.

[9]Cui C, Duan X, Collier B, Poduska KM. Fabrication and Wettability Analysis of Hydrophobic Stainless Steel Surfaces with Microscale Structures from Nanosecond Laser Machining *J. Micro Nano-Manuf.*. 2018;6:031006.

[10]Pan Y, Shi K, Duan X, Naterer GF. Experimental investigation of water droplet impact and freezing on micropatterned stainless steel surfaces with varying wettabilities *Int. J. Heat. Mass. Tran.*. 2019;129:953–964.

[11]Yoshimitsu Z, Nakajima A, Watanabe T, Hashimoto K. Effects of surface structure on the hydrophobicity and sliding behavior of water droplets *Langmuir*. 2002;18:5818–5822.

[12]Callies M, Quere D. On water repellency *Soft Matter*. 2005;1:55.

[13]Yuan Y, Lee TR. Contact angle and wetting properties *Springer Series in Surf. Sci.*. 2013;51:3-34.

[14]Gao Lichao, McCarthy Thomas J. Wetting 101° *Langmuir*. 2009;25:14105–14115.

[15]Hejazi V, Moghadam AD, Rohatgi P, Nosonovsky M. Beyond Wenzel and Cassie-Baxter: Second-order effects on the wetting of rough surfaces *Langmuir*. 2014;30:9423–9429.

[16]Guo P, Zheng Y, Wen M, Song C, Lin Y, Jiang L. Icephobic/Anti-Icing Properties of Micro/Nanostructured Surfaces *Adv. Mater.*. 2012;24:2642–2648.

[17]Barthwal S, Kim YS, Lim SH. Mechanically Robust Superamphiphobic Aluminum Surface with Nanopore-Embedded Microtexture *Langmuir*. 2013.

[18]Barthwal S, Lim SH. Fabrication of long-term stable superoleophobic surface based on copper oxide/cobalt oxide with micro-nanoscale hierarchical roughness *Appl. Surf. Sci.*. 2015;328:296–305.

[19]Xiang T, Zhang M, Li C, et al. A facile method for fabrication of superhydrophobic surface with controllable water adhesion and its applications *J. Alloy. Compd.*. 2017;704:170–179.

[20]Shi Z, Zhang X. Contact angle hysteresis analysis on superhydrophobic surface based on the design of channel and pillar models *Mater. Design*. 2017;131:323–333.

[21]Ma M, Hill RM. Superhydrophobic surfaces *Curr. Opin. Colloid. In.*. 2006;11:193–202.

[22]Extrand CW, Kumagai Y. An Experimental Study of Contact Angle Hysteresis *J. Colloid. Interf. Sci.*. 1997;191:378–383.

[23]Li P, Xie J, Deng Z. Characterization of irregularly micro-structured surfaces related to their wetting properties *Appl. Surf. Sci.*. 2015;335:29–38.

[24]Elms J. Characterizing dynamic wetting behaviour on irregularly roughened surfaces Master's thesisMemorial University of NewfoundlandSt. John's, NL (Canada) 2018.

[25]Furmidge CGL. Studies at phase interfaces. I. The sliding of liquid drops on solid surfaces and a theory for spray retention *J. Coll. Sci.*. 1962;17:309–324.

[26]Gulec S, Yadav S, Das R, Bhave V, Tadmor R. The Influence of Gravity on Contact Angle and Circumference of Sessile and Pendant Drops has a Crucial Historic Aspect *Langmuir.* 2019;35:5435–5441.

[27]Sakai M, Song JH, Yoshida N, Suzuki S, Kameshima Y, Nakajima A. Relationship between sliding acceleration of water droplets and dynamic contact angles on hydrophobic surfaces *Surf. Sci.*. 2006;600.

[28]Sakai M, Hashimoto A, Yoshida N, Suzuki S, Kameshima Y, Nakajima A. Image analysis system for evaluating sliding behavior of a liquid droplet on a hydrophobic surface *Rev. Sci. Instrum.*. 2007;78:45103.

[29]Pierce E, Carmona FJ, Amirfazli A. Understanding of sliding and contact angle results in tilted plate experiments *Colloid. Surf. A.*. 2008;323:73–82.

[30]Ravi Annapragada S, Murthy JY, Garimella SV. Prediction of droplet dynamics on an incline *Int. J. Heat Mass. Tran.*. 2012;55:1466–1474.

[31]Gao N, Geyer F, Pilat DW, et al. How drops start sliding over solid surfaces *Nat. Phys.*. 2018;14:191–196.

[32]Eral HB, 'T Mannetje D J CM, Oh J M. Contact angle hysteresis: A review of fundamentals and applications *Colloid. Polym. Sci.*. 2013;291:247–260.

[33]Krasovitski B, Marmur A. Drops down the hill: Theoretical study of limiting contact angles and the hysteresis range on a tilted plate *Langmuir.* 2005;21:3881–3885.

[34]ElSherbini AI, Jacobi AM. Retention forces and contact angles for critical liquid drops on non-horizontal surfaces *J. Colloid Interf. Sci.*. 2006;299:841–849.

[35]Makkonen L. A thermodynamic model of contact angle hysteresis *J. Chem. Phys.*. 2017;147:64703.

[36]Minghao R, Chengxia Y, Yuan F, et al. Model for rolling angle *J. Phys. Chem. C.* 2012;116:8449–8455.

[37]Xie J, Xu J, Shang W, Zhang K. Mode selection between sliding and rolling for droplet on inclined surface: Effect of surface wettability *Int. J. Heat Mass. Tran.*. 2018;122:45–58.

TABLE I: Comparison of acceptable measurements, as a function of data fitting rates, during volume modification contact angle measurements of 20 µL droplets.

Rate (s^{-1})	Acceptable	Total	%
1	7	15	48
2	106	252	42
3	2	15	13
4	3	15	20
5	4	15	27
10	3	15	20
as fast as possible	4	15	27

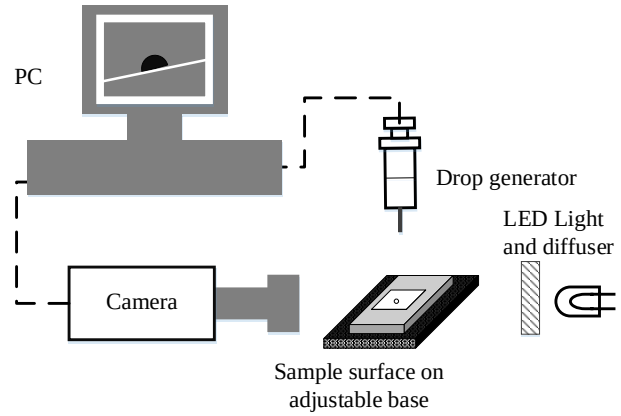

FIG. 1: Schematic diagram of the dynamic contact angle measurement setup. The adjustable base can be horizontal or tilted to facilitate either volume modification or sliding experiments, respectively.

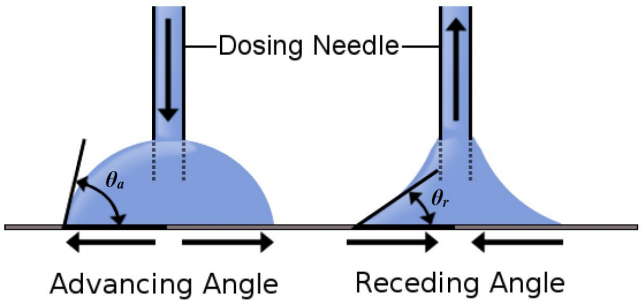

(a) Volume modification (horizontal surface)

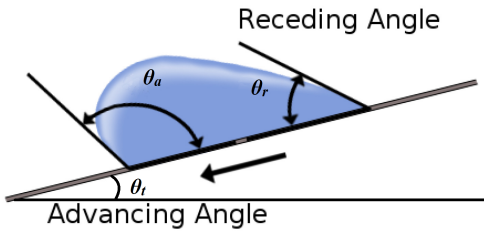

(b) Sliding (inclined surface)

FIG. 2: Schematic diagrams of two methods to assess dynamic contact angles: (a) droplet volume modification on horizontal surfaces, and (b) sliding droplets on inclined surfaces. The diagrams are adapted from thesis work.[24]

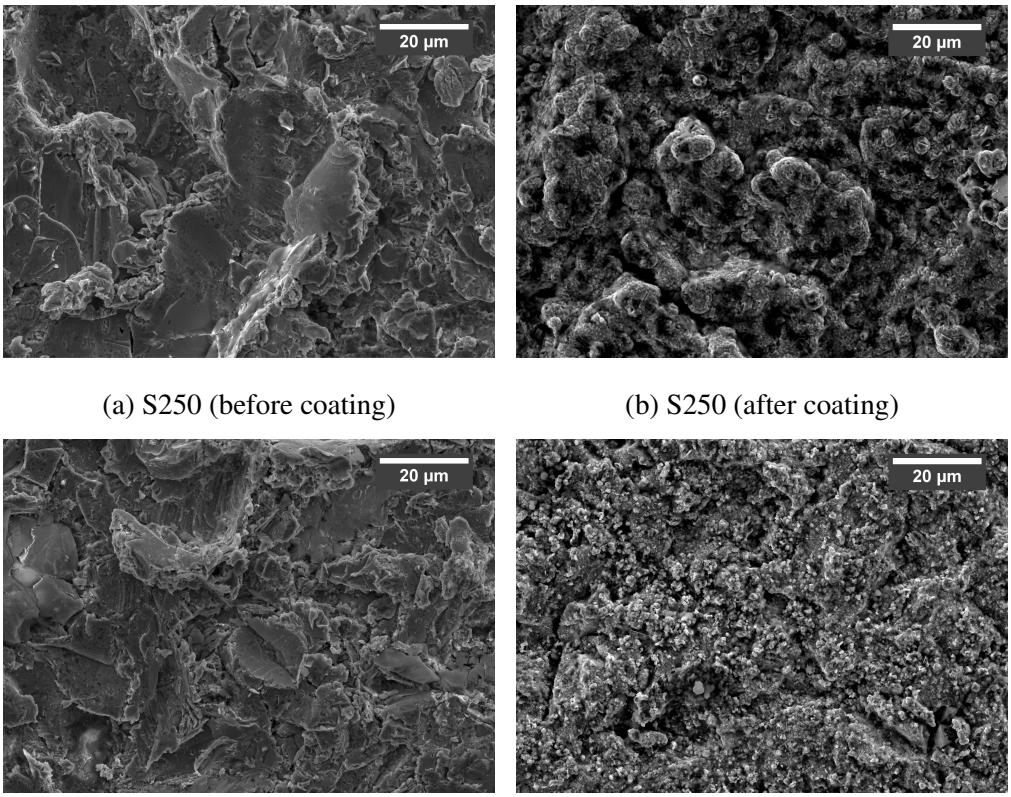

(a) S250 (before coating)

(b) S250 (after coating)

(c) S100 (before coating)

(d) S100 (after coating)

FIG. 3: Representative scanning electron micrographs of substrates(a,c) after sandblasting alone, or (b,d) after sandblasting, Zn electrodeposition, and stearic acid coating. Panels (a,b) show a sample that used 250 μm blasting media (labelled S250), while panels (b,d) show a sample prepared with 100 μm blasting media (labelled S100).

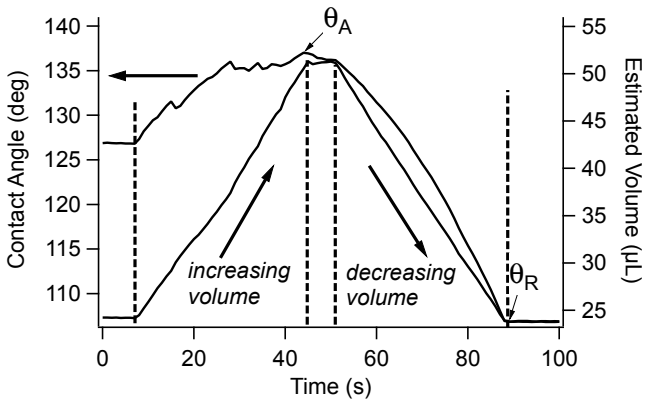

(a) contact angle data and estimated drop volume

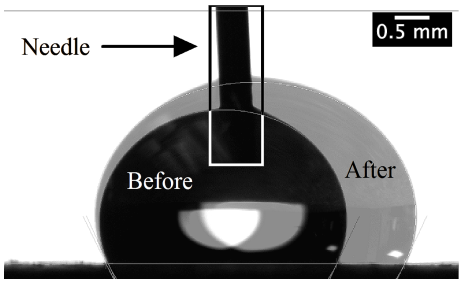

(b) droplet images before and after volume change

FIG. 4: (a) Representative contact angle data and estimated volume changes (extracted from fits of droplet images) for a volume-modified droplet on a sandblasted stainless steel surface. The droplet volumes and flow rates are user-programmed values (here, changing volume from 20 μL to 40 μL and back at 2 μL/s); the estimated volume changes plotted here are based on droplet cross-sectional areas calculated from images. In this case, the estimated droplet volume follows the actual (user-programmed) values quite well. (b) Representative example of asymmetry during the advancing phase of a volume-modified droplet. The black region corresponds to the initial droplet (needle centered), and the grey region shows the volume increase occurs preferentially to the right side of the droplet. These plots and images are adapted from thesis work.[24]

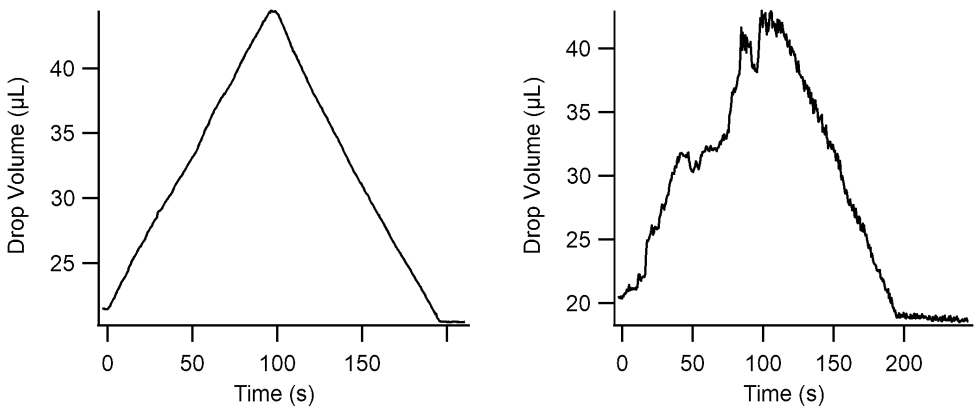

FIG. 5: Representative estimated droplet volumes as a function of time, calculated from fits of droplet cross-sectional images, for two different during dynamic measurements (20 µL initial volume, with an experimentally regulated volume change rate of 0.2 $\mu L s^{-1}$). Panel (a) shows smooth calculated volume changes that are consistent with the actual volume changes, while panel (b) shows an irregular trend that signifies poor fits to the droplet shape. These plots are adapted from thesis work.[24]

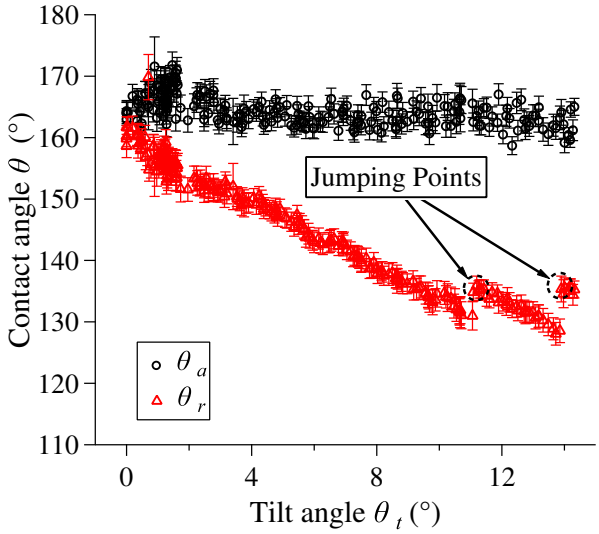

FIG. 6: Representative advancing (θ_a, black circles) and receding (θ_r, red triangles) contact angles as a function of increasing substrate tilt angle (θ_t), shown here for sample S100. Discontinuities in the contact angle trend are labelled as jumping points.

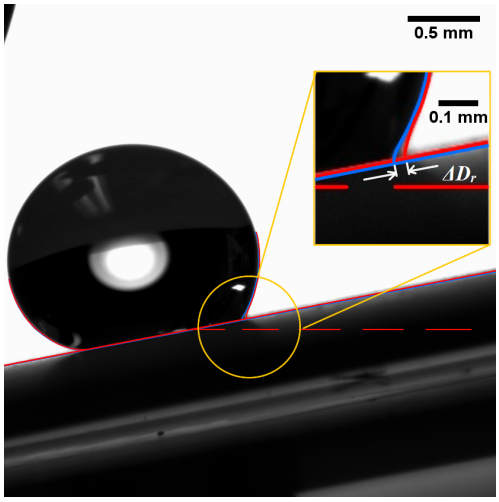

(a) Partial depinning

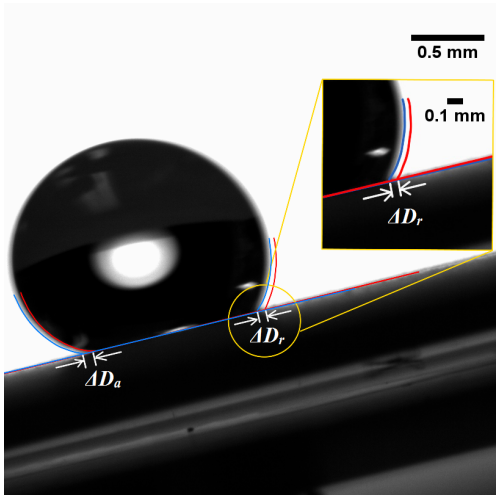

(b) Sliding

FIG. 7: Representative examples of a droplet on an inclined surface with (a) partial depinning and (b) sliding that correspond to the discontinuities circled on the plot in Figure 6.

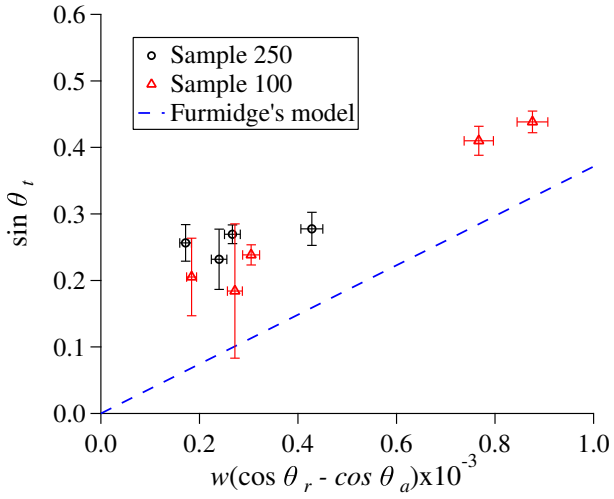

FIG. 8: Critical tilt angles from experiments plotted as a function of the predicted values from the Furmidge model (Equation 1), for two different samples.